The impact of the OSIRIS grating efficiency on radiance and trace-gas retrievals

C.A. McLinden, J.C. McConnell, K. Strong, I.C. McDade, R.L. Gattinger, R. King, B. Solheim, E.J. Llewellyn, and W.J.F. Evans

Abstract: The optical spectrograph and infrared imaging system (OSIRIS), launched in 2001, is a UV–visible diffraction-grating instrument designed to measure light scattered from the Earth's limb. Laboratory measurements of the OSIRIS diffraction-grating efficiency reveal a sensitivity to polarization including an anomalous structure of width 20–30 nm introduced into light polarized in a direction perpendicular to the grooves of the grating. A vector radiative-transfer model was used to generate synthetic OSIRIS spectra in an effort to examine the effect of this on radiances and trace-gas retrievals. Radiances that included grating effects were found to deviate by nearly 10% from those that did not and also contained the anomalous structure. Performing differential optical absorption spectroscopy (DOAS) on these spectra revealed errors in ozone apparent column densities of up to 80 DU. The size of the error was controlled mainly by the difference in polarization between the two DOAS spectra. Two possible correction methods were investigated. The first was to remove the grating effects by applying a correction factor to the raw radiances calculated using the vector radiative-transfer model. The second was to include the efficiency coefficient spectra in the DOAS fit.

PACS Nos.: 42.68Mj, 98.55Qf

Résumé : Le spectrographe optique et le système d'imagerie infrarouge OSIRIS est basé sur un réseau de diffraction UV–visible pour mesurer la lumière diffusée par le limbe terrestre. Les tests en laboratoires sur le rendement du réseau d'OSIRIS révèlent une sensibilité à la polarisation, incluant une structure anomale de largeur 20–30 nm pour la lumière polarisée dans la direction perpendiculaire aux rainures du réseau. Nous avons utilisé un modèle

Received 13 May 1999. Accepted 23 November 2001. Published on the NRC Research Press Web site at http://cjp.nrc.ca/ on 22 March 2002.

C.A. McLinden.[1,2] Department of Physics and Astronomy, York University, Toronto, ON M3J 1P3, Canada.
J.C. McConnell and I.C. McDade. Department of Earth and Atmospheric Science, York University, Toronto, ON M3J 1P3, Canada.
K. Strong. Department of Physics, University of Toronto, Toronto, ON M5S 1A7, Canada.
R.L. Gattinger and E.J. Llewellyn. Department of Physics and Engineering Physics, University of Saskatchewan, Saskatoon, SK S7N 5E2, Canada.
R. King. Institute for Space Research, University of Calgary, Calgary, AB T2N 1N4, Canada.
B. Solheim. Centre for Research in Earth and Space Science, York University, Toronto, ON M3J 1P3, Canada.
W.J.F. Evans. Department of Physics, Trent University, Peterborough, ON K9J 7B8, Canada.

[1]Corresponding author (e-mail: chris.mclinden@ec.gc.ca).
[2]Present Address: Meteorological Service of Canada, Downsview, ON M3H 5T4, Canada.

 DOI: 10.1139/P01-151

de transfert radiatif vectoriel pour générer des spectres synthétiques d'OSIRIS dans le but d'étudier les effets sur la radiance et la détermination des éléments présents sous forme de trace. Les valeurs de radiance qui incluent les effets du réseau peuvent dévier par 10% des valeurs qui ne les incluent pas, en plus de contenir des structures anomales. L'utilisation de la spectroscopie optique différentielle (DOAS) sur ces spectres révèle des erreurs dans la concentration apparente de la colonne d'ozone pouvant aller jusqu'à 80 DU. La grandeur de l'erreur est surtout due à la différence en polarisation entre les deux spectres DOAS. Nous étudions deux méthodes possibles de correction. La première corrige les effets particuliers du réseau en appliquant un facteur de correction aux radiances brutes calculées en par le modèle de transfert radiatif vectoriel. La deuxième introduit les spectres des coefficients de rendement dans la détermination par DOAS.

[Traduit par la Rédaction]

1. Introduction

It is in the nature of a diffraction grating to introduce an anomalous structure into diffracted spectra due to the complex interactions between the incident and diffracted fields and the grating surface [1]. Thus, spectra from any atmospheric sensor that employs a diffraction grating will contain these anomalies, which, if not accounted for, may potentially contaminate any quantity derived from them.

One such sensor is the optical spectrograph and infrared imaging system (OSIRIS) that measures sunlight scattered from the Earth's limb over a range of tangent heights from 280–450 nm at 1 nm resolution and from 450–800 nm at 2 nm resolution [2,3]. It is one of two instruments on the Odin satellite, which was launched in February 2001 into a circular, Sun-synchronous, near-terminator orbit at an altitude of approximately 600 km and an inclination angle of 97.8° [3].

Through the inversion of OSIRIS radiances, information on the abundance of important trace gases including O_3, O_4, NO_2, BrO, and OClO will be derived. However, with their small abundances, the spectral signature of these absorbers will represent only a small fraction of the total signal. Thus, spectral anomalies (or ghosts) such as those introduced by the diffraction grating may potentially lead to nontrivial errors in the retrieved quantities. It is the goal of this paper to

(1) characterize these anomalies in terms of location, magnitude, and shape,

(2) estimate the errors introduced if the anomalies are unaccounted for, and

(3) devise and evaluate possible methods of correction.

2. Efficiency-weighted radiance

2.1. Wood's anomalies

As first observed by R.W. Wood in 1902, the efficiency of any diffraction grating exhibits spectral anomalies in the form of rapidly varying peaks and troughs that arise from the complex interactions between the electromagnetic fields of the incident and diffracted waves and the surface of the grating [1,4]. Moreover, it is well known that these anomalies are polarization sensitive. For incident light with the electric field polarized perpendicular to the grooves of the grating, the anomalies possess much greater structure.

A qualitative understanding of why these anomalies arise can be gained from an explanation first put forth by Rayleigh, who suggested that they occur when the diffraction angle is 90°, a condition that occurs for a particular order at the so-called Rayleigh wavelength [1]. The energy in this order has to be redistributed into other orders and this accounts for the fluctuations of the efficiency. If the grating is a good conductor, it cannot sustain an electric field in the grating surface. Thus, the field strength of light polarized parallel to the grating grooves experiencing 90° diffraction (where the oscillations occur through the plane of the grating) will be much smaller than that of the light polarized perpendicular to the grating grooves (where the oscillations occur through the thickness of the grating). This means less energy needs to be redistributed and the anomalies are less severe in the light polarized parallel to the grating grooves. Accurate, quantitative prediction of grating efficiency is possible but this requires

Fig. 1. Schematic representation of the OSIRIS diffraction grating and its orientation relative to the parallel (∥) and perpendicular (⊥) components of the Stokes vector.

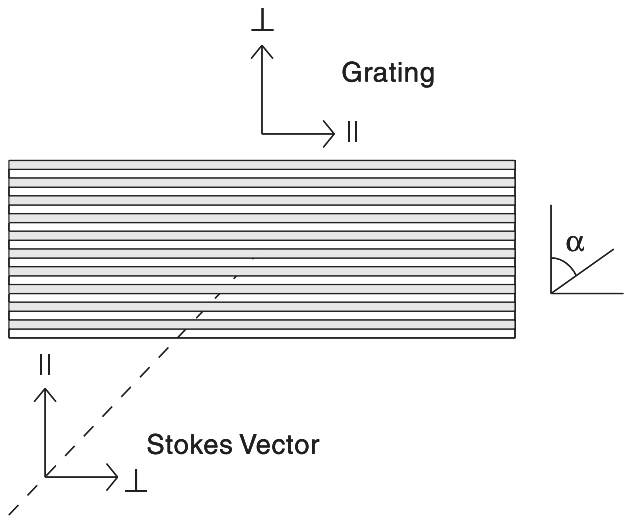

vector diffraction theory, which accounts for the shape and blazing, finite size, finite conductivity, and coating material of the grating.

Scattered sunlight will always have a nonzero component polarized perpendicular to the grooves. However, the relative strengths of the two components are variable and depend on the wavelength, the relative positions of OSIRIS and the Sun, the tangent height, and the state of the atmosphere. While one primary objective of OSIRIS is in the retrieval of vertical number-density profiles of some important trace species using their absorption features, it is essential that these anomalous efficiency features are known and accounted for.

2.2. Efficiency measurements

The radiation field incident on the diffraction grating is described in terms of the Stokes vector, $\boldsymbol{I} = [I \;\; Q \;\; U \;\; V]^{\mathrm{T}}$, a 4×1 column matrix written here as the transpose (superscript T) of a row matrix for convenience. Each element of the Stokes vector has units of radiance and collectively they describe the total radiance (I) and state of polarization (Q — linearly polarized light in a direction parallel and perpendicular to a reference plane, U — linearly polarized light in a direction 45° and 135° to a reference plane, and V — circularly polarized light). The reference plane is the meridian plane, which is defined by the local vertical and the direction of propagation. The grating is oriented such that the radiance component polarized parallel to its grooves corresponds to the perpendicular component relative to the meridian plane. This is shown in Fig. 1. Aligning the components requires a 90° rotation of the Stokes vector, which is accomplished through multiplication by a diagonal transformation matrix of elements $[1, -1, -1, 1]$ so that $\boldsymbol{I}' = [I \;\; -Q \;\; -U \;\; V]$. Figure 1 also defines an arbitrary direction that makes an angle α with the direction perpendicular to the grooves.

The radiance polarized parallel and perpendicular to the grooves of the grating is given by

$$I_{\parallel} = \frac{I - Q}{2}, \qquad I_{\perp} = \frac{I + Q}{2} \tag{1}$$

The fraction of light linear polarized, LP, is defined by

$$LP = \frac{\sqrt{Q^2 + U^2}}{I} \tag{2}$$

$$2\chi = \tan^{-1}\left(\frac{U}{Q}\right) \tag{3}$$

Fig. 2. Variation of the relative grating response with angle of polarization, α, for two pixels: # 357 (410 nm) and # 1100 (700 nm). Shown for each pixel are laboratory data (symbols) and a linear regression fit to the data (lines). Fits have functional form $(1 - 0.099\cos 2\alpha - 0.002\sin 2\alpha)$ for # 357 and $(1 + 0.021\cos 2\alpha - 0.011\sin 2\alpha)$ for # 1100.

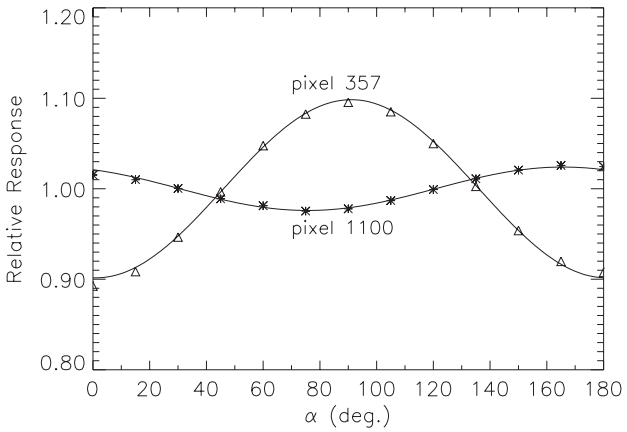

while χ denotes the angle of polarization. Hence, $Q = I \cdot LP\cos 2\chi$ and $U = I \cdot LP\sin 2\chi$.

The response of the grating is represented by a 4×4 linear transformation matrix, $\boldsymbol{G}$, so the diffracted radiance is given by matrix product $\boldsymbol{G}\,\boldsymbol{I}'$. The use of a linear transformation is justified as optical elements cannot introduce nonlinear effects at visible and near-visible wavelengths. As we are only interested in the total radiance of the diffracted light, only the top row of $\boldsymbol{G}$ is relevant. Furthermore, V is neglected as circularly polarized light in the terrestrial atmosphere is very small [5,6]. If the three elements comprising the top row of $\boldsymbol{G}$ are $[f \;\; fg_{12} \;\; fg_{13}]$ then the diffracted radiance, $I_{\rm dif}$, can be expressed as

$$I_{\rm dif} = f(\lambda)[1 \;\; g_{12}(\lambda) \;\; g_{13}(\lambda)][I \;\; -Q \;\; -U]^{\rm T} = f(\lambda)[I - g_{12}(\lambda)Q - g_{13}(\lambda)U] \tag{4}$$

The first element, f, represents the flat-field response of the grating, or the response to unpolarized light (i.e., $Q = U = 0$). The remaining two elements describe the modulation of the grating efficiency as a function of the linear polarization elements Q and U. All are functions of wavelength, λ.

If a polarizing filter oriented at angle α (defined above) is placed between the source and OSIRIS, and if the source consists of unpolarized light of unit intensity, $[1 \;\; 0 \;\; 0]^{\rm T}$, the diffracted light is then

$$\begin{aligned} I_{\rm dif}(\alpha) \;\; &\propto \;\; \left[\begin{array}{ccc} 1 & g_{12}(\lambda) & g_{13}(\lambda) \end{array}\right] \left[\begin{array}{ccc} 1 & \cos 2\alpha & \sin 2\alpha \\ \cos 2\alpha & \cos^2 2\alpha & \cos 2\alpha \sin 2\alpha \\ \sin 2\alpha & \cos 2\alpha \sin 2\alpha & \sin^2 2\alpha \end{array}\right] \left[\begin{array}{c} 1 \\ 0 \\ 0 \end{array}\right] \\ &= \;\; 1 + g_{12}(\lambda)\cos 2\alpha + g_{13}(\lambda)\sin 2\alpha \end{aligned} \tag{5}$$

where the 3×3 matrix is the transformation matrix for a polarizing filter (to within a constant) [7]. By rotating the polarizers (i.e., varying α) g_{12} and g_{13}, which are independent of the absolute response, can be deduced for each pixel through a multilinear regression.

As part of an overall OSIRIS flight-model-characterization effort, a suite of measurements designed to quantify g_{12} and g_{13} for each CCD pixel was performed at the University of Calgary. The experimental set-up consisted of an unpolarized light source incident on an integrating sphere with a polarizing filter placed between it and OSIRIS. Two sources were used: an uncalibrated 30 W quartz tungsten halogen (QTH) lamp and a 7 W calibrated QTH lamp. CCD images were made using exposure times of 0.01 to 0.3 s. Subtracted from each exposure was a dark-count image. The polarizer was rotated in 15° increments between $\alpha = 0$ and $\alpha = 180°$. Averaging was performed over 143 spatial pixels into 2, 4, 8, 16 and 32 bins. For the results presented here, the 32 bin averages were used and then co-added. The two polarizers used were a Melles Griot 03FPG011 dichroic sheet with an effective passband from 350–650 nm and an ORIEL 27320 with a passband from 230–770 nm.

Fig. 3. The OSIRIS grating efficiency parameters (*a*) g_{12} and g_{13} and (*b*) absolute calibration to sources polarized parallel and perpendicular to the grating grooves obtained by multiplying the absolute calibration to unpolarized light by $(1 - g_{12})$ (parallel) and $(1 + g_{12})$ (perpendicular).

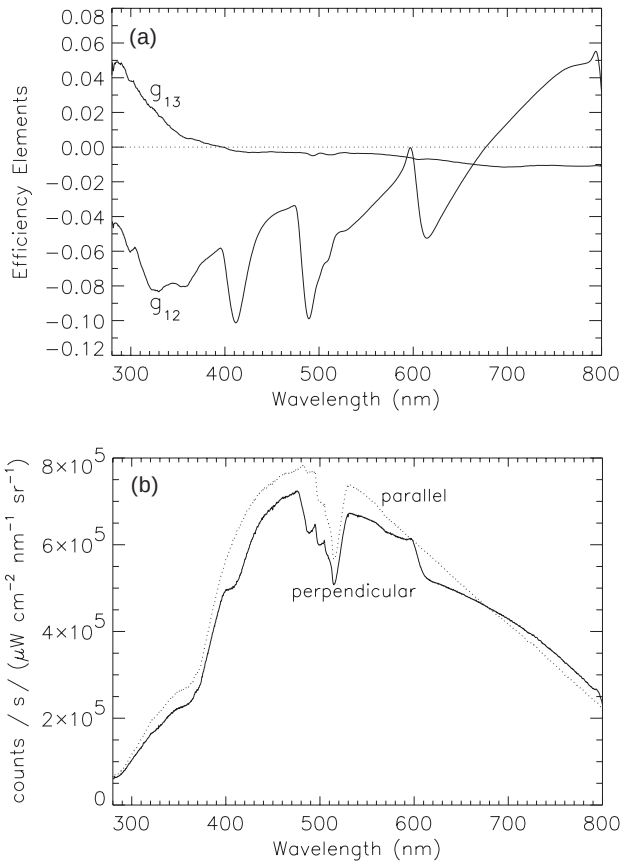

Data obtained using a combination of lamps, polarizers, and exposure times were found to give similar results with the largest differences being 2–4%. Sample data and linear regression fits for pixels 357 (∼400 nm) and 1100 (∼700 nm) are shown in Fig. 2. Clearly, the functional form of (5) is able to accurately and completely describe the data. We also note that g_{12} and g_{13} can be determined simply by evaluating the ratios

$$g_{12} = \frac{I_{\text{dif}}(0°)/I_{\text{dif}}(90°) - 1}{I_{\text{dif}}(0°)/I_{\text{dif}}(90°) + 1}, \qquad g_{13} = \frac{I_{\text{dif}}(45°)/I_{\text{dif}}(135°) - 1}{I_{\text{dif}}(45°)/I_{\text{dif}}(135°) + 1} \tag{6}$$

Again, these gave essentially the same results but were somewhat noisier.

The grating matrix elements g_{12} and g_{13} are plotted in Fig. 3*a* as a function of wavelength. Several distinct features are observed in g_{12} each with a width of about 20–30 nm and an amplitude of 0.05–0.08. The element g_{13} is generally smaller and possesses less structure. Note that the output of the QTH lamp falls off significantly below 350 nm and so the efficiency elements, or parameters, in this region are subject to much larger uncertainties.

Absolute calibration of OSIRIS to an unpolarized source has been carried out using a combination of the calibrated 7 W QTH lamp (>350 nm) and a calibrated deuterium lamp (<350 nm) [8]. In addition to the flat-field efficiency, f, this depends on the reflectivities of the mirrors and coatings, the efficiency of the order sorter, and the quantum yield of the detectors [2,9]. In Fig. 3*b*, the absolute calibration is shown for light polarized parallel and perpendicular to the grooves. These curves are obtained by multiplying the calibration for an unpolarized source by $g_{\parallel} = 1 - g_{12}$ for parallel-polarized light and

Table 1. OSIRIS geometries and calculated polarization. Given are day of year, locations of OSIRIS on that day, the solar zenith angle (θ_o), change in azimuthal angle ($\phi - \phi_o$), single-scattering angle (Θ_{ss}), polarization angle (χ), model-calculated average linear polarization (over a limb scan) at 500 nm and an albedo of 0.3 (LP), the analogous linear polarization but considering only radiances polarized parallel and perpendicular to the meridian plane (LP_Q), and the single-scattering linear-polarization ($LP_{Q,ss}$) (see Appendix A).

Day of year	Location of subtangent point		θ_o (°)	$\phi - \phi_o$ (°)	Θ_{ss} (°)	χ (°)	LP	LP_Q	$LP_{Q,ss}$
Summer solstice	Ascending equator	SAE	90.0	58.7	58.7	0.0	0.54	0.54	0.55
	Highest N. latitude	SHN	58.7	90.0	90.0	30.7	0.70	0.33	0.44
	Descending equator	SDE	90.0	121.3	121.3	0.0	0.54	0.54	0.55
Fall equinox	Ascending equator	FAE	90.0	82.3	82.3	0.0	0.89	0.89	0.91
	Highest N. latitude	FHN	82.3	90.0	90.0	7.5	0.85	0.82	0.91
	Descending equator	FDE	90.0	97.7	97.7	0.0	0.88	0.88	0.91
Terminator	Any	TER	90.0	90.0	90.0	0.0	0.92	0.92	0.95

by $g_\perp = 1 + g_{12}$ for perpendicular-polarized light. Much of the structure present in the perpendicular calibration curve is absent in the parallel one, as expected, based on the theory behind Wood's anomalies [1]. Using these definitions, (4) can be rewritten as

$$I_{\text{dif}} = f(\lambda)[g_\parallel(\lambda) I_\parallel + g_\perp(\lambda) I_\perp - g_{13}(\lambda)\, U] \tag{7}$$

2.3. Calculation of efficiency-weighted radiances

The radiative-transfer model of McLinden et al. [6] is used to calculate limb radiances, including linear polarization, for different Odin geometries. Each is defined in terms of a solar zenith angle at the tangent point (θ_o) and a change in azimuthal angle at the tangent point ($\phi - \phi_o$) and are functions of season, latitude of the subsatellite point, inclination of the orbit, and time of day. Three days are considered: summer solstice, fall equinox, and when the Odin ground track coincides with the terminator, which occurs in February and October. On each day, three points in the orbit are considered: when Odin ascends the equator (crosses the equator moving north), the highest northern latitude of the orbit, descending the equator (crossing the equator moving south). The highest southern latitude is not used as the Sun is well below the horizon at these points. The geometry for each scenario is given in Table 1. Note that when the orbit is along the terminator, the solar zenith angle and change in azimuthal angle are always 90°. The suite of geometries considered represents extremes of the Odin orbit in terms of the solar zenith angle and the scattering angle — factors that influence polarization.

To understand how and to what extent the grating efficiency impacts radiances, diffracted radiances as defined in (4) are compared with their unpolarized equivalents, which are obtained by setting $Q = U = 0$ and so are independent of g_{12} and g_{13}. These are referred to, respectively, as polarized and unpolarized radiances. Each was calculated using all geometries given in Table 1 for tangent heights between 10 and 70 km and from 280 to 800 nm in 0.5 nm increments [6]. An additional geometry in which the Sun is below the horizon is also used ($\theta_o = 93°$ and $\phi - \phi_o = 90°$; referred to as "SZA93"). For simplicity, a single, pure-Rayleigh atmosphere (May, 45°N) is used for all Odin geometries [6] and, unless otherwise specified, an albedo of 0.30 is used. As aerosols tend to depolarize scattered light, a pure-Rayleigh atmosphere should give the largest differences between the polarized and unpolarized radiances.

An example of polarized and unpolarized radiances are shown in Fig. 4*a* (with the latter offset for clarity) for fall equinox – ascending equator, or FAE, geometry (see Table 1) at a tangent height of 20 km. No obvious efficiency effects can be seen on the absolute radiances. The influence of the grating efficiency can be better examined through the ratio of polarized to unpolarized radiances. This is shown

Fig. 4. OSIRIS radiances (*a*) polarized (i.e., $I + g_{12}Q + g_{13}U$) and unpolarized (i.e., I) using FAE geometry at a tangent height of 20 km and a surface albedo of 0.3 and (*b*) ratio of polarized to unpolarized radiances for SAE, SHN, and TER geometries at a tangent height of 20 km and a surface albedo of 0.3.

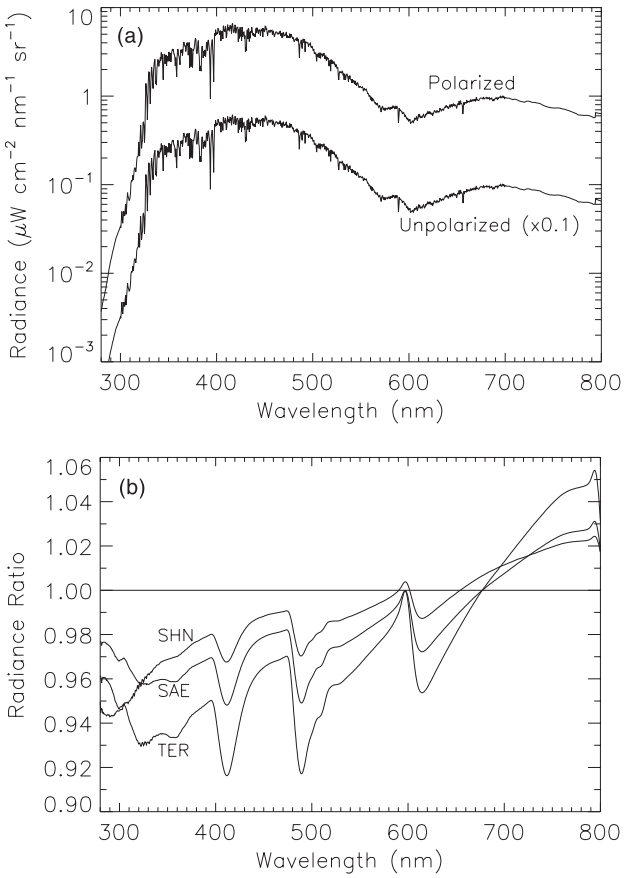

in Fig. 4*b* for SAE, SHN, and TER geometries, each at a tangent height of 20 km. The effect is clear and the structure generally mimics that of g_{12}. For cases when U is nonzero such as SHN, the effect of g_{13} is also evident at shorter wavelengths.

Polarization, as defined in (2), is given in Table 1 at 500 nm for each geometry as a mean value over the 10–70 km tangent-height range. Somewhat unexpectedly, the deviation of the radiance ratio from unity does not strictly correspond to polarization. This is explained as follows: if the polarization has a large contribution from radiances polarized at angles of 45° and 135° to the meridian plane (i.e., U is large and Q is small), there is reduced effect on the radiances owing to the relative magnitudes of g_{12} and g_{13}. Thus, an alternative definition of polarization is adopted that depends only on light polarized parallel and perpendicular to the grating,

$$LP_Q = \left|\frac{Q}{I}\right| = LP\cos 2\chi \tag{8}$$

Polarization as defined by (8) is also given in Table 1 and better corresponds to the deviation from unity of the radiance ratio.

3. Impact of efficiencies on DOAS apparent column densities

Trace-gas vertical number-density profiles will be used to recover the OSIRIS limb radiances in a two-step process. The first step uses the technique of differential optical absorption spectroscopy

(DOAS) that yields trace-gas apparent column densities (ACDs). The ACD represents the pathlength of the sunlight as it propagates through the atmosphere weighted at each point with the local number density. DOAS requires taking the ratio of two spectra: one in which the light has passed through a large amount of the absorber being recovered and one in which the light has passed through little (referred to as the reference spectrum). In DOAS, the high-frequency (or differential) components of the individual absorption cross sections are used as basis functions and fitted via least squares to the measured differential optical depth, which is obtained by taking the log-ratio of the spectra. The fitted coefficient of each absorber represents the difference in ACD between that in the two spectra. Greater detail of the DOAS technique as applied to OSIRIS measurements can be found elsewhere [9,10].

In the second step, ACDs are related to the vertical number-density profiles through a weighting-function matrix. This matrix describes how the local densities at each altitude contribute to the ACD observed for a given tangent height [10]. The elements of such a matrix are not simple geometric factors as is the case for solar occultation. Rather, the complexity and combinations of paths require these elements be calculated using a radiative-transfer model. Two retrieval methods are in development for use on OSIRIS measurements optimal estimation [9] and an iterative least-squares algorithm [10].

This study does not address the impact of the Wood's anomalies on the retrieved profiles; our focus is the impact on ACDs. Towards that end, DOAS is performed on synthetic (or model generated) spectra using a 450–550 nm fitting window [9]. This region is useful for the retrieval of ozone and NO_2 although O_4 (a short lived O_2–O_2 collision complex) also possess absorption features in this region. A DOAS fit to polarized radiances is shown in Fig. 5. In this example, the spectrum is obtained using TER geometry at a tangent height of 30 km while the reference was obtained using SAE geometry at a tangent height of 70 km. While the general features of the measured differential optical depth are captured in the fit, there are significant deviations near 470 and 490 nm. The reason for this large difference is due to the additional structure introduced by the Wood's anomalies that has not been accounted for. Also shown in Fig. 5 is the residual of the fit, or the difference between the measured and fitted differential optical depths. It is, on average, about 25% of the total differential optical depth. In addition, the measured and fitted ozone, NO_2, O_4, and Rayleigh (see Strong et al. [9]) differential optical depths are shown in Figs. 5*c*– 5*f*. Each of these are obtained by subtracting the differential optical depth of all other absorbers from both the total measured and fitted differential optical depth. Large differences between the fitted and measured differential optical depth are evident in each.

To quantify the errors introduced by the Wood's anomalies, DOAS was performed on synthetic polarized and unpolarized radiances using selected geometries from Table 1. The ACD obtained using the unpolarized radiances is taken as the "true" or exact value as it does not contain any grating terms. For each geometry and tangent height, the difference in ACD between that using the polarized and unpolarized radiances is computed and is taken as the grating-induced error. Initially, the reference spectrum is taken as the 70 km radiance from that scan. In this case the difference in ACD was found to be small, less than 10 DU. This small effect can be explained in terms of the small difference in polarization between the two DOAS radiances. At 450–550 nm, polarization varies less than 0.04 between any two tangent heights for the same geometry.

However, the top step in a given scan is usually not used as the reference. Instead, a spectrum obtained over a region of low albedo and (or) at a smaller solar zenith angle is often used to ensure the smallest absorption signature possible in the reference spectrum. ACDs were recalculated using the SHN 70 km radiances (where the solar zenith angle is 58.7°, a minimum for the Odin orbit) as the reference spectrum for all other scan geometries. ACDs for selected geometries are shown in Fig. 6*a*. Negative values at large tangent heights indicate a greater absorption signature in the reference spectrum (recall ACD actually represents the difference in the apparent column densities between the two spectra). ACD errors are shown in Fig. 6*b* and are much larger (5–80 DU). The magnitude of the differences follows the difference in LP_Q between that of the scan geometry and that of the SHN reference geometry from Table 1. This implies that the larger the offset in polarization between the two radiances, the larger the grating-induced errors in the ACDs. The values of $LP_{Q,\mathrm{ss}}$ roughly follow this same trend but, as they do not account for multiple scattering and surface reflection, are only approximate.

The effect of a highly reflecting surface was also investigated by regenerating TER spectra with an albedo of 0.8. The ACD errors were reduced slightly with the larger albedo as this tends to depolarize the light and thus it more closely matched the polarization of the SHN reference. Increased depolarization

Fig. 5. Summary of DOAS fit: (*a*) measured (continuous line) and fitted (broken line) differential optical depth and (*b*) the fit residual. The remaining panels display the measured (continuous line) and fitted (broken line) differential optical depth for (*c*) ozone, (*d*) NO_2, (*e*) O_4, and (*f*) Rayleigh. (Spectrum: FDE, albedo of 0.3, tangent height of 30 km; Reference: SHN, albedo of 0.3, tangent height of 70 km).

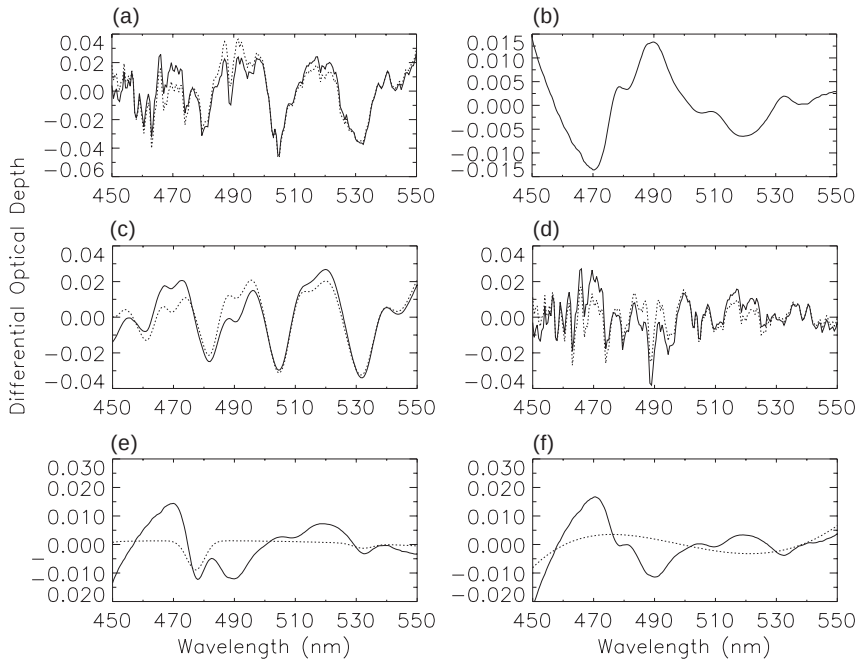

occurs as surface-reflected light is scattered into the OSIRIS line of sight over a large range of scattering angles.

Efficiency-induced errors in NO_2 ACDs tend to be larger, typically by a factor of 1–4. The reason for this is unclear and somewhat counter-intuitive as the greater structure of the NO_2 cross sections should mean it is less sensitive to the broader efficiency features. In addition to 450–550 nm, a 340–390 nm DOAS fitting window will be used for the retrieval of O_3, NO_2, BrO, and OClO [10]. From Fig. 3*a*, the efficiency features in this region are smaller, which should result in smaller errors although this needs to be verified with additional modelling. Also, greater multiple scattering at these wavelengths will tend to decrease the differences in polarization between the various geometries.

4. Efficiency corrections

The ideal method of accounting for the effects of the grating efficiency would be to correct the raw radiances to prevent any errors from propagating into the data products derived from them. This can be done by converting the measured polarized radiance into an equivalent unpolarized radiance. Such a correction factor, C, is simply the ratio of the two

$$C(\lambda) = 1 - g_{12}(\lambda)\frac{Q}{I} - g_{13}(\lambda)\frac{U}{I} = 1 - LP[g_{12}(\lambda)\cos 2\chi + g_{13}(\lambda)\sin 2\chi] \tag{9}$$

This factor has both a grating dependence and polarization dependence. It becomes unity only for unpolarized light or $g_{12} = g_{13} = 0$. As C represents the ratio of the two radiances, Fig. 4*b* is actually showing $C(\lambda)$ vs. wavelength for the different geometries.

The correction factor of (9) is similar to that used for processing the global ozone-monitoring experiment (GOME) data [11] although the GOME correction does not include a g_{13} term as $U = 0$ for nadir viewing (but is nonzero for off-nadir viewing). GOME makes broadband measurements of LP for wavelengths longer than 300 nm while for shorter wavelengths, single-scattering model calculations

Fig. 6. (*a*) Ozone apparent column densities (ACDs) for indicated geometries using SHN, albedo of 0.3, tangent height of 70 km as reference; (*b*) error introduces into ACDs by not accounted for efficiency structures; (*c*) error remaining in ACDs after includes differential efficiencies in DOAS fit. In each panel the dotted line is for TER geometry using an albedo of 0.8.

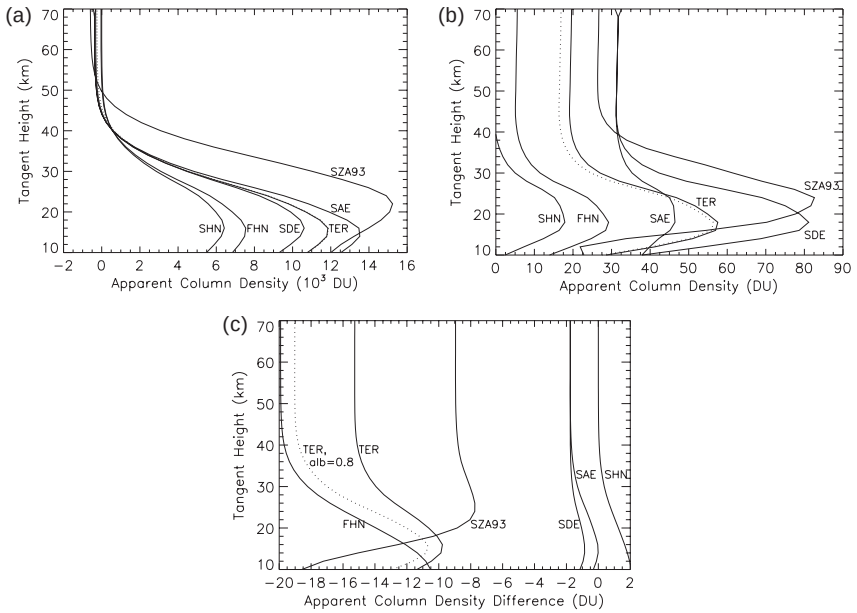

are used. OSIRIS will not make any separate polarization measurements and so if this type of approach is to be used, it would be necessary to use modelled values for LP and χ. Note that this correction factor is exact as long as LP and χ are known exactly. However, due to the inherent limitations of a one-dimensional radiative transfer model and uncertainties in input parameters such as surface albedo and model atmosphere, this is not possible. An estimate of how uncertainties in LP lead to errors in C can be obtained using

$$\left|\frac{\Delta C}{C}\right|_{\max} \approx 0.1|\Delta LP| \tag{10}$$

where ΔLP is the uncertainty in polarization and $\chi = 0$ and $g_{12} = 0.1$ (from Fig. 3*a*) were used to obtain a maximum. Thus, for a maximum error in C of 1%, LP needs to be known to 0.1 or better. This seems achievable using single-scattering values for LP and χ (see Appendix A) with tabulated corrections for multiple scattering, albedo, aerosols, etc. Alternatively, look-up tables for LP itself could be created. This approach is facilitated as polarization in the visible generally changes slowly with tangent height and wavelength [6] so that values need only be tabulated every 50 nm or so (upward of 350 nm) and at tangent heights of 10, 20, 30, and 60 km. An important exception to this is in the O_2 or H_2O bands [12].

An alternative method of accounting for the anomalous efficiency features is to include differential efficiencies in the least-squares fit to the measured spectra, where the differential efficiencies are the high-frequency components of g_{12} and g_{13}. In effect, efficiency is treated as a pseudo-absorber analogous to how the Ring effect [13] is often handled in DOAS [14]. This method has the disadvantage of being empirical (and hence approximate) and also does not actually correct the measured radiances. Its main advantage is that it does not require any model calculations and so is not subject to the uncertainties associated with them.

As an illustration, the DOAS fit of Fig. 5 was repeated, including differential spectra for both g_{12} and g_{13}, with the results shown in Fig. 7. The overall and individual fits match the measurements very closely with the residual reduced by a factor of 25 and the ACD error is now about 2 DU. Differences

Fig. 7. Summary of DOAS fit including differential grating efficiencies. (*a*) Measured (continuous line) and fitted (broken line) differential optical depth and (*b*) the fit residual. The remaining panels display the measured (continuous line) and fitted (broken line) differential optical depth for (*c*) ozone, (*d*) NO_2, (*e*) O_4, (*f*) Rayleigh, (*g*) measured (continuous line) and fitted (broken line) differential optical depths for differential g_{12} spectrum, and (*h*) measured (continuous line) and fitted (broken line) differential optical depths for differential g_{13} spectrum. Note the change in scale in panel (*b*) from that in Fig. 5. (Spectrum: FDE, albedo of 0.3, tangent height of 30 km; Reference: SHN, albedo of 0.3, tangent height of 70 km.) The broken lines are not visible in (*a*), (*c*), and (*d*) because they are superimposed on the continuous line, and are just visible in (*e*)–(*g*).

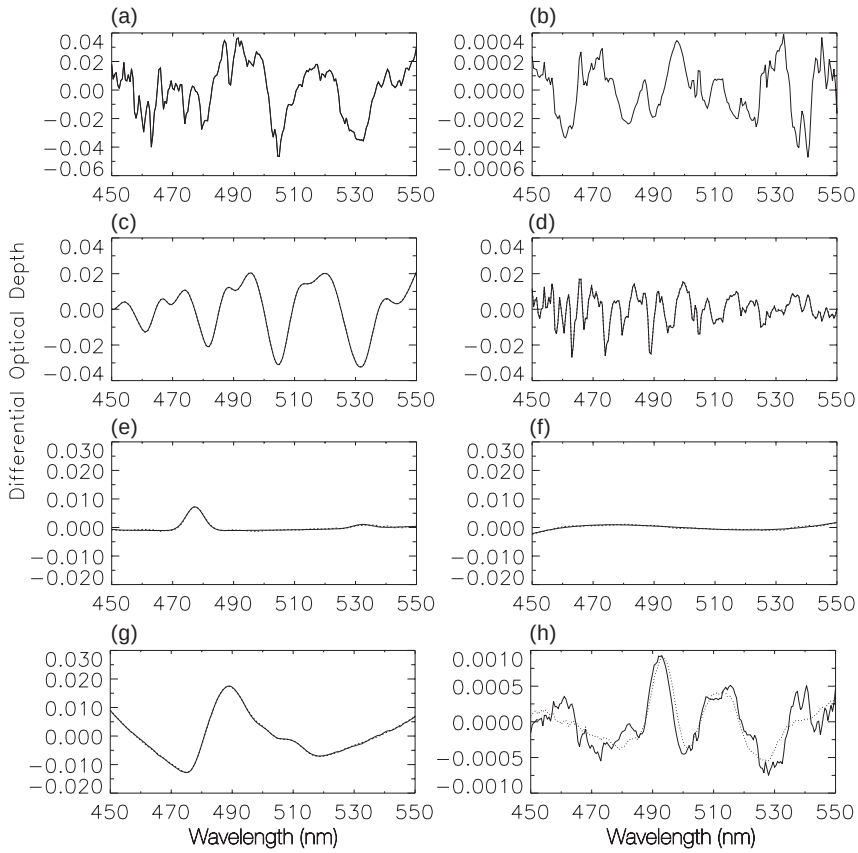

in ACD when including efficiency in the DOAS fit are shown in Fig. 6*c* and should be compared with those in Fig. 6*b*. The errors now vary from 0–20 DU, a reduction by roughly a factor of 5.

The size of the fitted efficiency differential optical depths contain information on the difference in polarization between the two radiances used in the DOAS fit. If the polarization of the reference can be obtained via modelling, it should be possible to infer the polarization of the second spectrum. This can then be used in lieu of a model-calculated polarization in the radiance correction factor. Such a possibility is currently being explored [15].

The two correction schemes outlined above can be used together, either in parallel or in series. Using them in parallel allows for an ACD consistency check as each should yield (approximately) the same answer. Using the two in series would enable any residual structure in the DOAS fit that was not removed after applying the radiance correction factor to be accounted for.

5. Conclusions

The OSIRIS diffraction grating responds differently to incident light polarized parallel and perpendicular to the grooves of the grating. In particular, the grating introduces spectral anomalies of width

20–30 nm into perpendicular polarized light. The polarization response of the OSIRIS grating is described in terms of two parameters, g_{12} and g_{13}. These were determined experimentally for each pixel by examining the variation of the signal with the rotation of a polarizing filter.

A vector radiative-transfer model was used to calculate synthetic OSIRIS polarized radiances (which include grating efficiency) and unpolarized radiances (which do not include the grating efficiency) for several Odin geometries. Differences of nearly 10% were found. The effect of this anomalous structure on the DOAS ozone apparent column densities was assessed using a 450–550 nm spectral fitting window. When using a reference spectrum for a high-Sun geometry, errors of 5–80 DU resulted and can be traced to the difference in polarization of the two radiances used in the DOAS.

Two methods of correcting or accounting for the effects of the polarization-dependent efficiencies were investigated. The first is a correction factor applied to the raw radiances and is based on vector radiative-transfer model calculations of linear polarization and polarization angle. The second was to include a differential efficiency ratio spectrum in the DOAS fit, an empirical method. A combination of the two methods may be the most viable as any error in the radiance correction factor will lead to residual grating efficiency structure in the radiances. A study examining how the uncertainties in albedo, aerosol, and ozone profiles affect the radiance correction factor is planned.

Acknowledgements

The authors wish to acknowledge the Canadian Space Agency, the Natural Sciences and Engineering Research Council of Canada, and the Meteorological Service of Canada for continuing support.

References

1. M.C. Hutley. Diffraction gratings. Academic Press, London. 1982. pp. 165–193.
2. E.J. Llewellyn. Can. J. Phys. **80** (2002). This issue, the foreword.
3. D.P. Murtagh, U. Frisk, F. Merino et al. Can. J. Phys. **80** (2002). This issue.
4. S. Solimeno, B. Crosignani, and P. Di Porto. Guiding, diffraction, and confinement of optical radiation. Academic Press, London. 1986. pp. 418–419.
5. J.E. Hansen and L.D. Travis. Space Sci. Rev. **16**, 527 (1974).
6. C.A. McLinden, J.C. McConnell, E. Griffioen, and C.T. McElroy. Can. J. Phys. **80** (2002). This issue.
7. G.L. Stephens. Remote sensing of the lower atmosphere. Oxford Press, London. 1994. p. 64.
8. J. Stegman. Private communication, 1998.
9. K. Strong, B.M. Joseph, R. Dosanjh, I.C. McDade, C.A. McLinden, J.C. McConnell, J. Stegman, D.P. Murtagh, and E.J. Llewellyn. Can. J. Phys. **80** (2002). This issue.
10. I.C. McDade, K. Strong, C.S. Haley, J. Stegman, D.P. Murtagh, and E.J. Llewellyn. Can. J. Phys. **80** (2002). This issue.
11. P. Stammes, I. Aben, R.B.A. Koelemeijer, S. Slijkhuis, and D.M. Stam. GOME polarisation validation study. Proceedings of the 3rd Symposium on Space and the Environment, Florence, Italy. 17–21 March 1997. ESA SP-414, 669 (1997).
12. I. Aben, F. Helderman, D.M. Stam, and P. Stammes. Geophys. Res. Lett. **26**, 591 (1999).
13. J.F. Grainger and J. Ring. Nature, **193**, 762 (1962).
14. K. Chance and R.J.D. Spurr. Appl. Opt. **36**, 5224 (1997).
15. C. von Savigny. Private communication, 2000.

A. Appendix: Single scattering and polarization

As much of the radiance is scattered only once and by Rayleigh scatterers it is useful to examine some single-scattering quantities. We first define the single-scattering angle, Θ_{ss}, and the single-scattering polarization angle, χ_{ss}

$$\cos\Theta_{ss} = \sin\theta_o \cos(\phi - \phi_o) \tag{A.1}$$

$$\cos\chi_{ss} = \frac{\cos\theta_o}{\sin\Theta_{ss}} \tag{A.2}$$

where χ_{ss} depends only on the geometry. Note these are valid for limb viewing only ($\mu = 0$).

Based on these, the (Rayleigh) single-scattering polarization, LP_{ss}, and the single-scattering polarization parallel and perpendicular to the meridian plane, $LP_{Q,ss}$, are

$$LP_{ss} = \frac{\sin^2 \Theta_{ss}}{1.058 + \cos^2 \Theta_{ss}} \tag{A.3}$$

$$LP_{Q,ss} = \frac{\sin^2 \Theta_{ss}}{1.058 + \cos^2 \Theta_{ss}} \cdot \cos 2\chi_{ss} \tag{A.4}$$

These equations contain the well-known Rayleigh polarization [5] with 1.058 (at 500 nm) in place of 1.0 in the denominator to account for the anisotropy of the molecular scatterers [5,15]. The second factor in (A.4) ensures that only the parallel and perpendicular components contribute to the polarization. Values of $LP_{Q,ss}$ have been calculated for each geometry and are given in Table 1. Note that even for scattering angles of 90°, polarization as defined in (A.4) will be small if the solar zenith angle is near 45°. Finally, we note that multiple scattering acts to introduce only a small change in the ratio U/Q and so χ_{ss} is generally an excellent approximation to χ (i.e., much better than LP_{ss} is to LP).